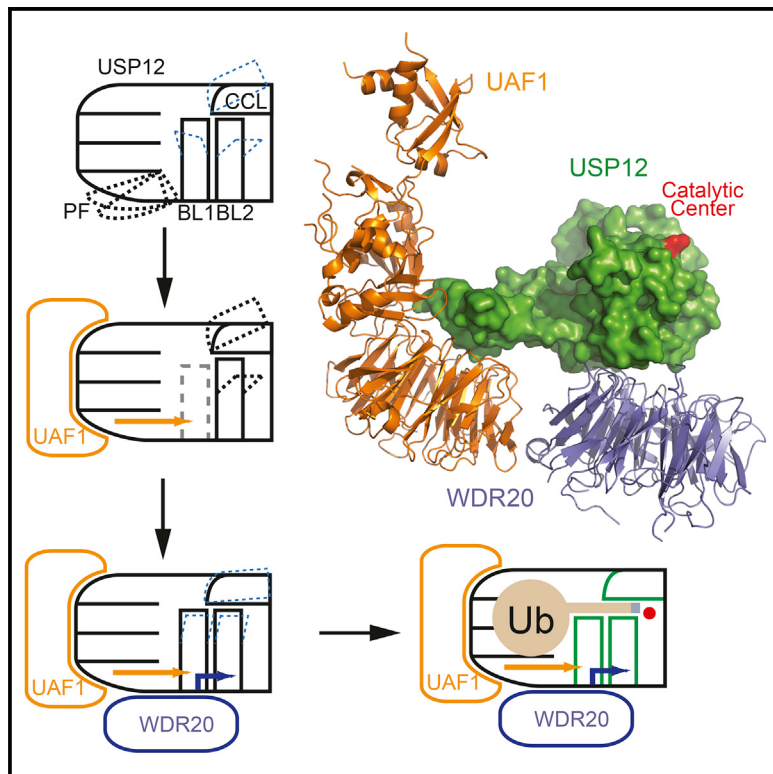


Molecular Cell

Allosteric Activation of Ubiquitin-Specific Proteases by β -Propeller Proteins UAF1 and WDR20

Graphical Abstract



Authors

Heng Li, Kah Suan Lim,
Hyungjin Kim, ..., Champak Chatterjee,
Alan D. D'Andrea, Ning Zheng

Correspondence

nzheng@uw.edu

In Brief

UAF1 and WDR20 are two β -propeller proteins capable of synergistically activating the deubiquitinase USP12. Li et al. report on the different binding modes of the two β -propeller proteins on USP12 and their distinct allosteric mechanisms for activating the deubiquitinating enzyme.

Highlights

- Free USP12 deubiquitinase is inactive and has several flexible structural elements
- UAF1 and WDR20 can both activate USP12 without increasing its substrate affinity
- UAF1 and WDR20 bind USP12 at two distinct sites away from its catalytic center
- Two distinct allosteric mechanisms underlie USP12 activation by UAF1 and WDR20

Accession Numbers

5K16
5K1B
5K1A
5K19
5K1C

Allosteric Activation of Ubiquitin-Specific Proteases by β -Propeller Proteins UAF1 and WDR20

Heng Li,^{1,3} Kah Suan Lim,⁴ Hyungjin Kim,⁵ Thomas R. Hinds,¹ Ukhyun Jo,⁵ Haibin Mao,^{1,3} Caroline E. Weller,² Ji Sun,¹ Champak Chatterjee,² Alan D. D'Andrea,⁴ and Ning Zheng^{1,3,*}

¹Department of Pharmacology

²Department of Chemistry

³Howard Hughes Medical Institute, Box 357280
University of Washington, Seattle, WA 98195, USA

⁴Department of Radiation Oncology, Dana-Farber Cancer Institute, Harvard Medical School, Boston, MA 02115, USA

⁵Department of Pharmacological Sciences, Stony Brook University, Stony Brook, NY 11794, USA

*Correspondence: nzheng@uw.edu

<http://dx.doi.org/10.1016/j.molcel.2016.05.031>

SUMMARY

Ubiquitin-specific proteases (USPs) constitute the largest family of deubiquitinating enzymes, whose catalytic competency is often modulated by their binding partners through unknown mechanisms. Here we report on a series of crystallographic and biochemical analyses of an evolutionarily conserved deubiquitinase, USP12, which is activated by two β -propeller proteins, UAF1 and WDR20. Our structures reveal that UAF1 and WDR20 interact with USP12 at two distinct sites far from its catalytic center. Without increasing the substrate affinity of USP12, the two β -propeller proteins potentiate the enzyme through different allosteric mechanisms. UAF1 docks at the distal end of the USP12 Fingers domain and induces a cascade of structural changes that reach a critical ubiquitin-contacting loop adjacent to the catalytic cleft. By contrast, WDR20 anchors at the base of this loop and remotely modulates the catalytic center of the enzyme. Our results provide a mechanistic example for allosteric activation of USPs by their regulatory partners.

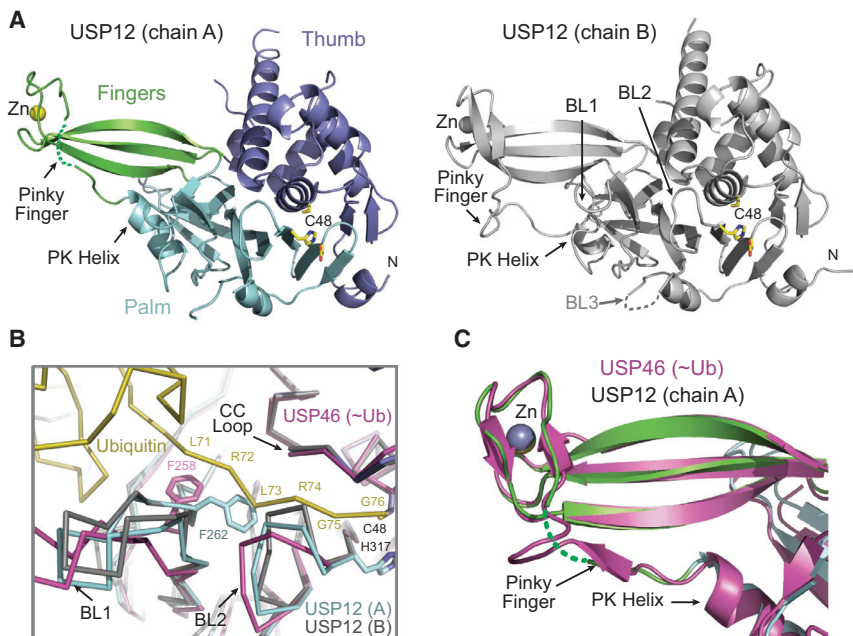
INTRODUCTION

Protein ubiquitination is a widespread form of post-translational modification (PTM) that regulates a range of cellular functions in eukaryotes (Hershko and Ciechanover, 1998). Central to this modification is the formation of a stable isopeptide bond between the ubiquitin (Ub) C terminus and a lysine residue of the target protein. Akin to other PTMs, ubiquitination is often reversible and can dynamically modulate the function and stability of the substrate proteins. Studies in the past two decades have identified a superfamily of deubiquitinating enzymes (DUBs) capable of cleaving the isopeptide bond between the Ub and the modified protein (Reyes-Turcu et al., 2009). Their isopeptidase activities are conferred by one of five unique catalytic do-

mains, which are used to classify these enzymes into five distinct families (Komander et al., 2009; Nijman et al., 2005b).

Ubiquitin-specific proteases (USPs) constitute the largest family of human DUBs, with at least 50 family members (Komander et al., 2009). By deubiquitinating specific protein substrates, USPs regulate a multitude of critical cellular processes, such as signal transduction, gene expression, DNA repair, and cell-cycle progression. As intracellular proteases, the proper functions of USPs require precise control of their catalytic competency and substrate specificity. Proteomics studies have identified distinct protein networks in which USP enzymes can perform their context-dependent cellular functions through protein-protein interactions (Sowa et al., 2009; Ye et al., 2009).

USP1, USP12, and USP46 represent a cohort of human DUBs whose catalytic activities are tightly controlled by a common binding partner. USP1, the founding member of this USP subfamily, plays an essential role in the Fanconi anemia (FA) DNA repair pathways by removing mono-Ub from FANCD2 and PCNA (Huang et al., 2006; Kim and D'Andrea, 2012; Moldovan and D'Andrea, 2009; Nijman et al., 2005a). However, USP12 and USP46 are two closely related DUBs responsible for deubiquitinating and stabilizing a variety of protein substrates in cell signaling (Burska et al., 2013; Dahlberg and Joo, 2014; Gangula and Maddika, 2013; Joo et al., 2011; Li et al., 2013; McClurg et al., 2014; Moretti et al., 2012). USP12 in particular is implicated in prostate cancer as a co-activator of the androgen receptor and is overexpressed in colorectal carcinoma driven by a focally amplified superenhancer (Burska et al., 2013; Zhang et al., 2016). Affinity-based analyses have identified an evolutionarily conserved WD40-repeat-containing protein, UAF1 (USP1-associated factor 1), which can directly interact with all three USPs (Cohn et al., 2007; Sowa et al., 2009). Although in isolation these three USP enzymes are mostly inactive, their isopeptidase activities are strongly enhanced upon binding to UAF1 (Cohn et al., 2009; Dahlberg and Joo, 2014; Gangula and Maddika, 2013). USP12 and USP46, but not USP1, can be independently activated by another WD40-repeat-containing protein, WDR20 (Burska et al., 2013; Dahlberg and Joo, 2014; Kee et al., 2010; McClurg et al., 2014). Together, UAF1 and WDR20 are able to synergistically stimulate the enzymatic activities of USP12 and USP46 to a peak level. UAF1 regulates these DUBs beyond simple enzyme activation.

**Figure 1. Structure of Free Human USP12**

(A) Overall fold of USP12 with the Thumb (slate), Palm (cyan), and Fingers (green) subdomains shown in a ribbon diagram, the zinc (yellow) in a sphere, and the catalytic triad in sticks. The dashed line indicates the flexible region of Pinky Finger. The second USP12 molecule (chain B) in the asymmetric unit is shown on the right, with the structurally different Pinky Finger and PK Helix highlighted.

(B) Superposition of the two free USP12 structures (cyan and gray) with Ub~USP46 (yellow and magenta, PDB: 5CVM) showing the narrow catalytic cleft of free USP12. The Thumb and Palm domains of the USPs are aligned through the $C\alpha$ atoms. The BL1 residue F262 of free USP12, which partially occupies the catalytic cleft, is shown in sticks. Its corresponding residue in USP46, F258, is also shown for contrast. Three enzyme loops contacting the Ub tail are labeled. The C-terminal LRGG motif of Ub accommodated by the catalytic cleft is indicated.

(C) The Fingers domain of free USP12 (chain A) and Ub~USP46 are superimposed to highlight their differences at the Pinky Finger region.

A C-terminal SUMO-like domain of UAF1 has been uncovered to mediate the recruitment of mono-ubiquitinated FANCD2 and PCNA substrate proteins to USP1 (Yang et al., 2011). UAF1, therefore, represents a prototypical USP regulator, which has two critical functions, enzyme activation and substrate recruitment, integrated into a single polypeptide.

Despite current advances in structural and biochemical studies of USPs, the mechanisms by which these important cellular enzymes are activated by their interacting partners remain elusive. Earlier structural analyses of USP catalytic domains in their free and Ub-bound forms have highlighted conformational changes associated with Ub binding at either the catalytic center or the Ub tail-binding cleft (Hu et al., 2002, 2005). But the question remains as to whether these substrate-induced changes are involved in USP activation by non-substrate regulatory partners. In a report, the crystal structures of free and UAF1-complexed USP46 have been determined with a conjugated suicidal Ub substrate (Yin et al., 2015). However, a structural comparison of the enzyme in these two post-reaction forms revealed few conformational differences, leaving the mechanism of USP46 activation by UAF1 elusive. To better understand enzyme activation without the interference from the suicidal substrate, we determined the crystal structures of Ub-free USP12 in isolated, UAF1-bound, and UAF1-WDR20-complexed forms. Our results not only unravel the allosteric nature of USP12 activation by the two WD40-repeat-containing proteins but also help dissect their discrete allosteric effects transmitted by pliable structural elements of USP12.

RESULTS

Structures of Inactive Free USP12

To gain structural insights into the inactive form of the enzyme, we first determined the structures of nearly full-length USP12

at a 2.6 Å resolution. USP12 was crystallized with two molecules in the asymmetric unit (Table S1). The enzyme adopts a canonical right-hand-like USP fold, which consists of three subdomains, Fingers, Thumb, and Palm (Figures 1A and S1A). Previous studies have shown that the Fingers domain of USPs is responsible for cradling the globular domain of Ub, whereas the Thumb and Palm domains flank a long and narrow catalytic cleft, recognizing the extended Ub tail and presenting its C terminus to the active site cysteine (Hu et al., 2002; Yin et al., 2015). Similar to most USPs of known structures, the active site of USP12 is in a catalytically competent conformation (Figure S1B), suggesting that its enzymatic activation does not involve major reorganization of the catalytic triad. Superposition analysis of USP12 with several Ub-bound USP structures, including Ub~USP46 and Ub~USP14, reveals a partially closed catalytic cleft of the free enzyme, which is constricted by two previously highlighted USP Palm domain surface loops, blocking loops (BLs) 1 and 2 (Figures 1B, S1C, and S1D) (Hu et al., 2005; Yin et al., 2015). To accommodate the Ub tail, these two loops would have to undergo conformational changes to make room for the substrate. Nevertheless, the free USP12 structure alone is insufficient to link these predicted changes to USP12 activation by UAF1 or WDR20.

From the two USP12 molecules in the asymmetric unit, the Fingers domain of the enzyme displays an unusual structural plasticity. In other known USP structures, the extended Fingers domain is defined by a four-stranded antiparallel β sheet, which is frequently stabilized by a zinc ion coordinated at the fingertip region (Figure 1C) (Avvakumov et al., 2006; Ernst et al., 2013; Hu et al., 2002; Köhler et al., 2010; Lei et al., 2014; Ratia et al., 2006; Renatus et al., 2006; Samara et al., 2010; Ye et al., 2011; Yin et al., 2015). Surprisingly, in one copy of USP12, no clear electron density is present for part of the sequence at the outer edge of the Fingers domain, which we name the Pinky Finger

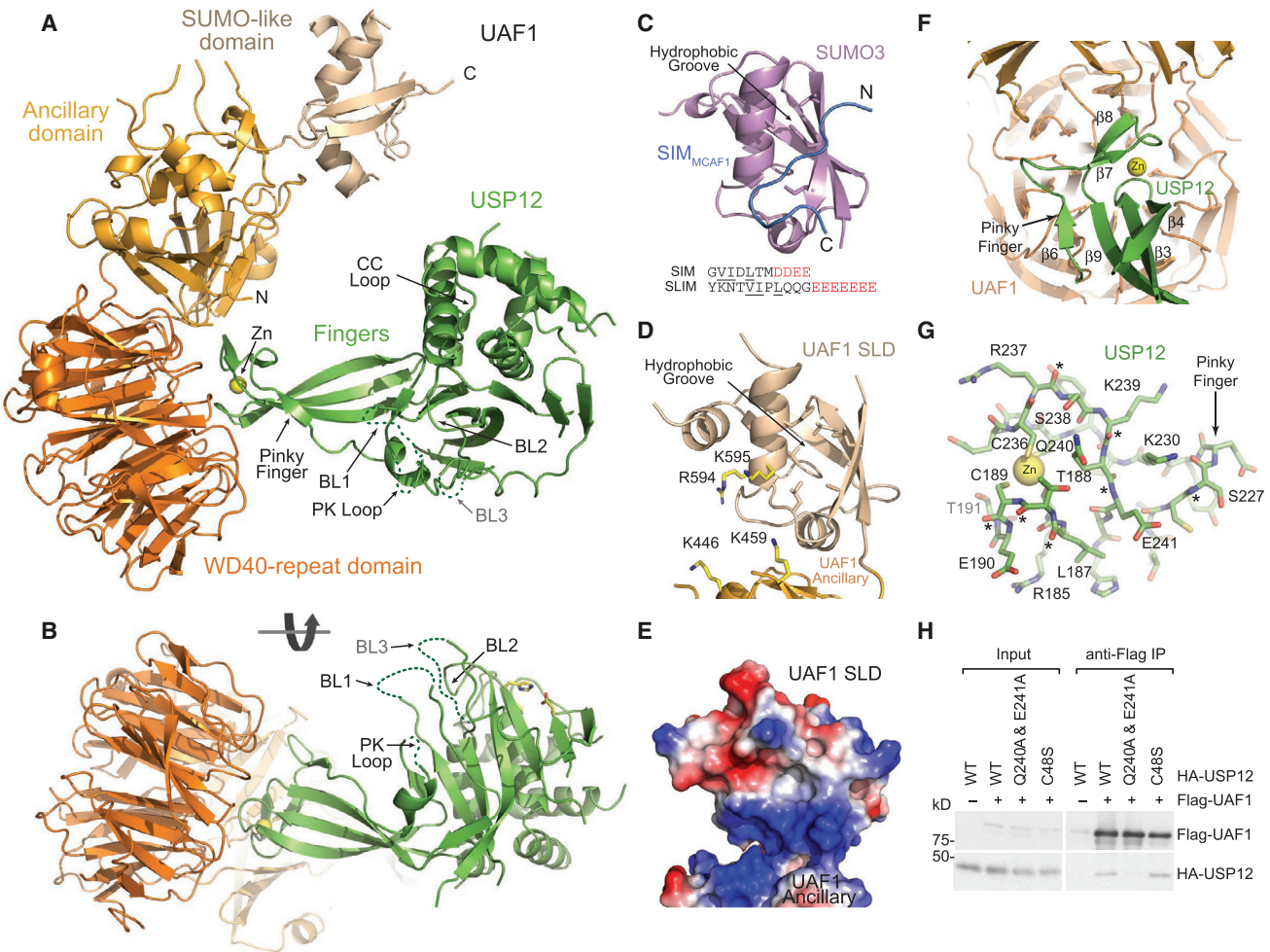


Figure 2. Overall Architecture of the UAF1-USP12 Complex

(A and B) Ribbon diagram of the UAF1-USP12 complex in two orthogonal views. USP12 is in green, and the three UAF1 domains are labeled and colored differently. The dashed lines represent disordered USP12 loops. The USP12 catalytic triad is shown in sticks.

(C) Overall structure of the SUMO3-SIM_{MCAF1} complex (PDB: 2RPQ) and the MCAF1 SIM and FANCI SLIM sequences. Characteristic hydrophobic and acidic residues of SIM and SLIM are underlined and in red, respectively.

(D) A close-up view of the UAF1 SUMO-like domain shown in the same orientation as in (C). Four basic UAF1 residues potentially responsible for recognizing the acidic tail of SLIM are shown in sticks.

(E) Electrostatic surface potential of UAF1 SLD.

(F) Ribbon diagram of the UAF1-USP12 interface viewed from the Thumb-Palm scaffold of the enzyme, with zinc shown as a yellow sphere. The β strands of the USP12 Fingers domain are labeled.

(G) The fingertip region of the USP12 Fingers domain viewed from UAF1, with UAF1-interacting residues labeled. Asterisks indicate backbone groups that are part of the intermolecular hydrogen bond network.

(H) Interactions of wild-type (WT) and mutant USP12 with UAF1 assessed by immunoprecipitation (IP) and western blot using an in vitro transcription and translation system.

(Figures 1A and 1C). In the other copy of USP12, the entire Pinky Finger sequence adopts a distinct coiled structure and is detached from the rest of the Fingers domain (Figures 1A and S1E). This large structural difference between the two copies of USP12 can be traced to an upstream α helix, which bridges the Fingers and Palm domains in the first molecule but is half-melted in the second copy (Figure 1A). We name this α helix the Proximal Knuckle (PK) Helix. Together, these unique features of the Ub-free USP12 structures hint at possible involvement of the USP12 Fingers domain in enzyme regulation.

UAF1-USP12 Complex Structure

To delineate the mechanism by which UAF1 activates USP12, we next determined the crystal structure of USP12 in a complex with full-length human UAF1 in the F222 space group at 3.2 Å (Table S1). Reminiscent of the Ub-bound UAF1-USP46 complex, the UAF1-USP12 structure features an L-shaped architecture, in which the elongated UAF1 protein packs perpendicularly against the DUB (Figures 2A and 2B). Different from the UAF1-USP46~Ub structure, the previously predicted C-terminal SUMO-like domain of UAF1 is clearly resolved in

the UAF1-USP12 complex, in addition to the N-terminal WD40-repeat domain and a central ancillary domain (Figures 2A, 2B, 2D, and S2A–S2E) (Yang et al., 2011).

SUMO is known to mediate protein interactions by recognizing a consensus SUMO-interacting motif (SIM) found in a variety of proteins (Hecker et al., 2006; Song et al., 2004). We have shown that the UAF1 SUMO-like domain (SLD) targets the FANCD2–FANCI heterodimer and the PCNA-hELG1 complex to USP1 by directly recognizing a SUMO-like domain-interacting motif (SLIM) in FANCI and hELG1 (Yang et al., 2011). A comparison of UAF1 with a documented SUMO3-SIM_{MCAF1} complex structure predicts that the UAF1 SLD recognizes SLIMs through an analogous binding mode, as found in the SUMO-SIM interaction (Figures 2C and 2D) (Sekiyama et al., 2008). Similar to SUMO, the UAF1 SLD features a hydrophobic groove between its central helix and the second β strand, which most likely recognizes the hydrophobic portion of SLIMs. Distinct from SUMO, however, the UAF1 SLD packs against the central ancillary domain. Together, they create a highly basic cleft, which is expected to house the long string of negatively charged residues in the C-terminal half of SLIMs (Figures 2C and 2E). In support of this notion, mutation of a single UAF1 lysine residue (K595) at the center of this predicted SLIM-binding site was sufficient to impair UAF1-hELG1 interaction (Yang et al., 2011).

As expected for two USPs with an 89% sequence identity, USP12 and USP46 share a binding mode similar to that of UAF1, which is mediated by the “top” surface of the UAF1 WD40-repeat β -propeller domain (Figures S2A and S3A). The UAF1-binding site on USP12 is exclusively confined at the tip region of its Fingers domain, which consists of a short loop linking the Middle and Index Fingers (β 3 and β 4) and a β hairpin connecting the Pinky and Ring Fingers (β 6 and β 9) (Figure 2F). These two structural elements are held together by a central zinc ion, which is coordinated by four cysteine residues conserved in many USPs. In contrast to UAF1, which recognizes the DUB with mostly its amino acid side chains (Figure S2F), USP12 contacts its activator via an approximately equal number of side chain and backbone interactions (Figure 3G). Only half of the USP12 residues at the interface are conserved among human USP12, USP46, and USP1, suggesting that their polypeptide backbone structure plays an important role in governing specific interactions with UAF1. We validated the UAF1-USP12 interface by mutating two neighboring residues (Q240 and E241) at the center of the USP12 fingertip region and two pairs of aromatic residues at the top surface of the UAF1 WD40-repeat domain (Figures 2F and S2F). All mutants impaired UAF1-USP12 complex formation (Figures 2H and S2G). Through similar mutational analyses, we confirmed that USP12 and USP1 share a similar UAF1-binding mode (Figure S2H).

Structural Comparison of Free and UAF1-Bound USP12

Few structural differences were previously detected in the post-reaction form of USP46 upon UAF1 binding (Yin et al., 2015). By contrast, a comparison between free and UAF1-bound USP12 structures without suicidal Ub unveils a concatenation of conformational differences spreading across the protein. Starting at the tip of the Fingers domain, the UAF1-USP12 interface directly stabilizes the distal region of the USP12 Pinky Finger (Figure 3A),

which is either disordered or in a different conformation in the two USP12-alone structures. This effect further converts the middle portion of the Pinky Finger into a regular β strand that completes the four-stranded β sheet of the Fingers domain (Figures 1C and 2A). In this remodeled conformation, the entire Pinky Finger sequence forms a long ladder of backbone hydrogen bonds with the Ring finger, which reaches all the way to the proximal ends of the two fingers (Figure 3B).

Through the Pinky Finger, the effect of UAF1 binding appears to further propagate into the USP12 Thumb-Palm scaffold via the PK Helix at the Fingers-Palm domain junction. In the free USP12 structures, the PK Helix shows two structural configurations in which Phe219, a residue strictly conserved among USP1, USP12, and USP46, is either embedded in a hydrophobic domain junction pocket or completely detached from the catalytic domain (Figure 3C). In the UAF1-USP12 complex structure, this aromatic residue is dislodged from the pocket but tucked underneath the Ring Finger between the side chains of Arg245 and Lys247 (Figure 3D). As a result, the PK Helix is pulled and locked into a new position, which leads to relaxation of its preceding loop, hereafter referred to as the PK Loop (Figure 3D). In both free USP12 structures, the PK Loop directly packs against and buttresses the base of the ~30-amino acid-long BL1 (Figure 3E). In contrast, the PK Loop in the UAF1-USP12 complex structure appears to adopt a flexible structure, as evidenced by the absence of its electron density. Concomitant with its structural disorganization, the nearby BL1 becomes destabilized, showing no electron density (Figure 3F).

To confirm that these structural differences of USP12 are associated with UAF1 binding but not crystal packing or resolution limit, we crystallized the UAF1-USP12 complex in another space group (C2) and determined its structure at a 2.3 Å resolution. The high-resolution complex structure determined in this new space group structure features the same cascade of conformational changes, spanning from the regularized Pinky Finger to the destabilized BL1, despite slightly varied curvature of the Fingers domain (Figure S3C). The only major differences between the two complex structures are found at the catalytic cleft (Figure 3G). Although the active site of USP12 in the UAF1-USP12 complex crystallized in F222 space group adopts the same topology as found in the free enzyme (Figure S3F), in the C2 space group structure, the USP12 Thumb domain features a series of major structural rearrangements at the catalytic cleft. These include (1) relocation of the sequence N terminus to the catalytic cysteine, (2) a large positional shift of the α 5 helix, and (3) complete destabilization of a loop outlining the catalytic cleft (α 6– α 7 loop), which was previously named the switching loop and is hereafter referred to as Catalytic Cleft Loop (CC Loop) (Figure 3G) (Faesen et al., 2011). These changes are accompanied by a large movement of BL2 on the Palm domain, which flips away from the Thumb domain by 180° and geometrically distorts the catalytic triad (Figure 3G). The catalytic cleft opened up by the movement of BL2 becomes partially occupied by the base of a loop between the two BLs, which we name BL3. Superposition analysis predicts that this third Palm domain loop is in collision with the Ub tail in the C2 space group UAF1-USP12 structure (Figure S3G). In the free USP12 structure and in the F222 space group structure of the UAF1-USP12 complex, this loop is

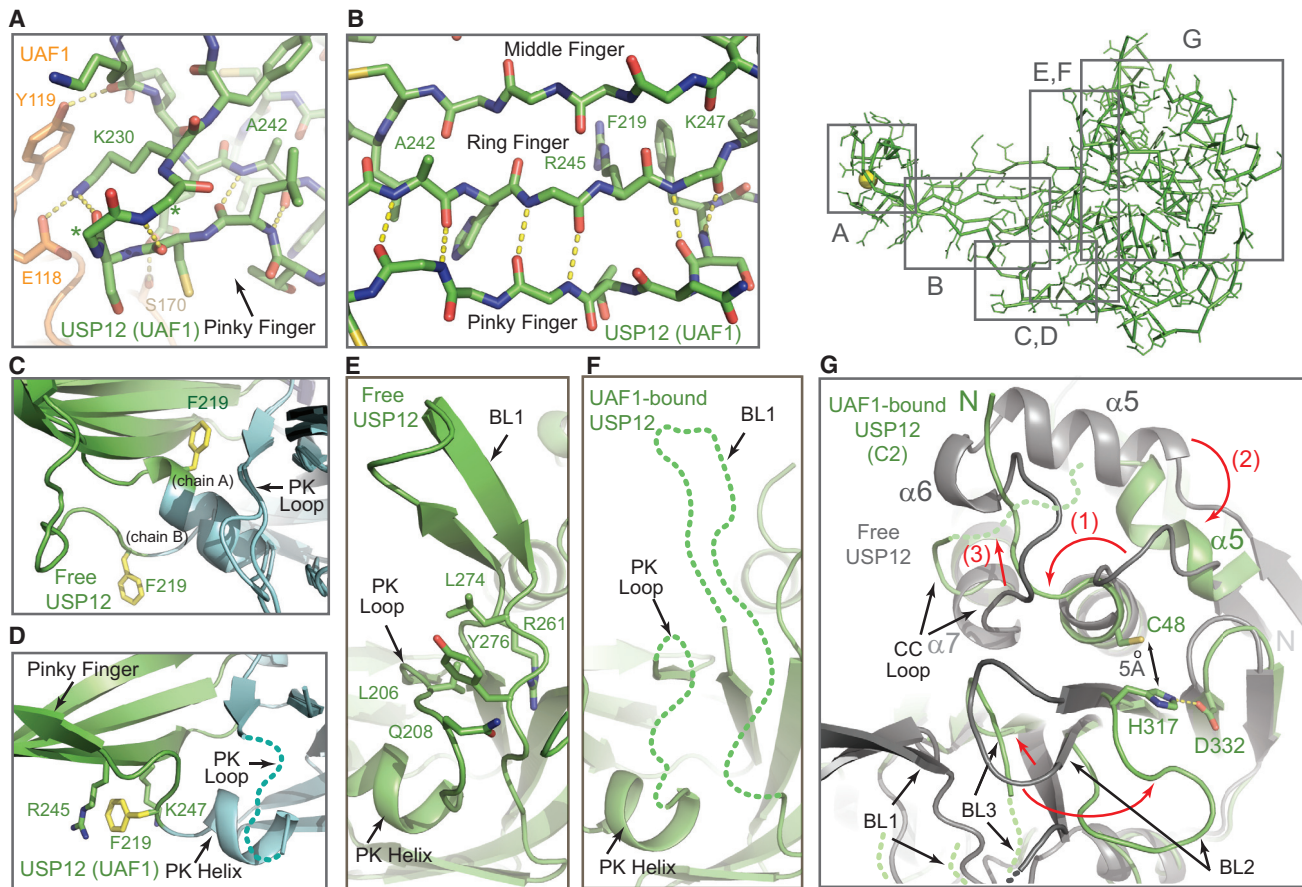


Figure 3. Structural Differences between Free and UAF1-Bound USP12

(A) Side view of the interface between UAF1 (orange) and the tip of USP12 Pinky Finger (green). Yellow dashed lines represent hydrogen bonds. The side chains of two amino acids labeled with asterisks are not involved in the interface and are omitted for clarity.

(B) A close-up view of the UAF1-stabilized backbone hydrogen bond network between the Pinky and the Ring Fingers of USP12.

(C and D) A close-up comparison of the Pinky Finger, PK Helix, and PK Loop between free and UAF1-bound USP12 structures, with the two free USP12 structures aligned in (C). The structurally regularized Pinky Finger in UAF1-bound USP12 is indicated in (D). F219 and its two interacting residues in the UAF1-bound USP12 structure are highlighted in sticks. The dashed line indicates the disordered PK Loop of UAF1-bound USP12. The Fingers and Palm domains of USP12 are in green and cyan, respectively.

(E and F) A close-up comparison of the PK Loop and BL1 between free and UAF1-bound USP12 structures. The dashed lines in (F) indicate the disordered PK Loop and BL1 in the UAF1-bound USP12 structure. The side chains of select amino acids involved in PK Loop and BL1 interactions are shown in sticks in (E).

(G) Superposition of the free and UAF1-bound USP12 structures focusing on the Palm domain, the catalytic cleft, BL2, and BL3. Green dotted lines represent disordered ends of polypeptide breaks in the UAF1-bound USP12 structure (determined in the C2 space group). Red arrows highlight large movements of secondary structure elements. Sticks show the disorganized catalytic center in the UAF1-bound USP12 structure.

excluded from the catalytic cleft by BL1 and BL2. Overall, our two UAF1-USP12 structures not only reveal a series of structural changes of the enzyme that are connected to the binding site of UAF1 but also highlight the dynamic nature of three key loops, namely, BL2, BL3, and the CC Loop, surrounding the catalytic site of the activated enzyme.

UAF1-USP12-WDR20 Complex Structure

To investigate the mechanism by which WDR20 activates USP12, we next determined the crystal structure of a ternary complex consisting of USP12, UAF1 lacking its SLD, and WDR20 at a 3.0 Å resolution (Table S1). WDR20 is predicted to be a single-domain protein with a β-propeller fold formed by WD40-repeat motifs. In the ternary complex, WDR20 is juxta-

posed with the WD40-repeat domains of UAF1 and closely engaged with the USP12 Palm domain (Figure 4A). Just like UAF1, WDR20 is strikingly far removed from the USP12 active site. The closest distances between the USP12 catalytic cysteine and the two activating proteins, WDR20 and UAF1, are about 20 and 40 Å, respectively. Despite a potential salt bridge and a small number of van der Waal interactions between the two β propellers, UAF1 binding to USP12 has little effect on the association of WDR20 with the enzyme (Figures S4A and S4B).

Similar to the UAF1 WD40-repeat domain, WDR20 folds into a seven-bladed β propeller and interacts with USP12 through its top surface (Figures 4B and S4C). The overall size of the WDR20 β propeller is larger than that of UAF1 due to several

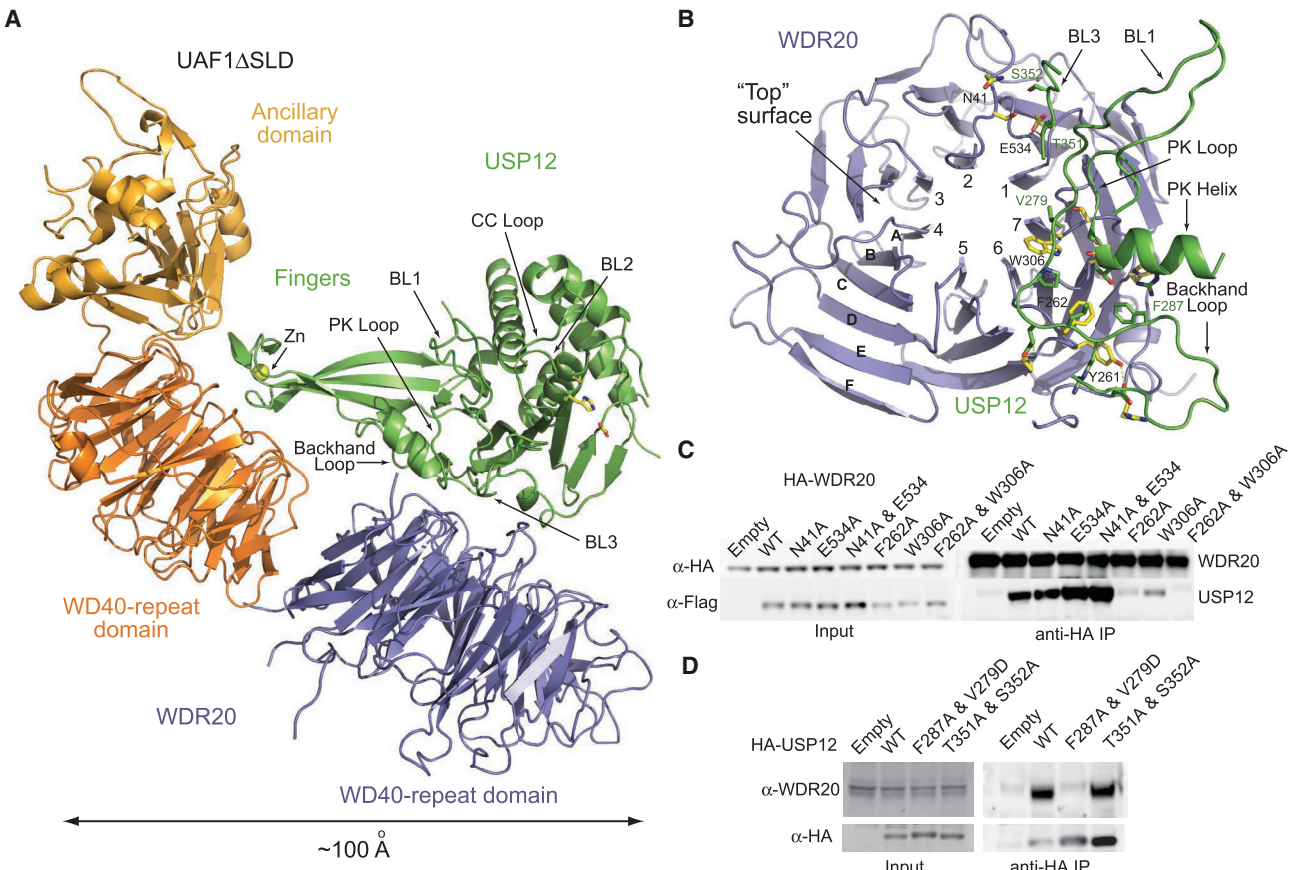


Figure 4. Crystal Structure of a UAF1-USP12-WDR20 Complex

(A) Ribbon diagram of the UAF1 Δ SLD-USP12-WDR20 complex with WDR20 shown in a slate color and the catalytic triad in sticks. (B) A close-up view of the top surface of the WDR20 propeller domain, with USP12-interacting residues shown in sticks. The seven blades are numbered 1 to 7. The six β strands in the fourth blade are labeled A to F. USP12 structural elements involved in binding WDR20 are shown in a ribbon diagram without the rest of the enzyme for clarity. Key WDR20-interacting residues in USP12 are shown in sticks. (C) Interactions of FLAG-tagged wild-type (WT) and mutant WDR20 with HA-tagged USP12 are assessed by immunoprecipitation (IP) and western blot upon co-transfection. (D) Interactions of HA-tagged WT and mutant USP12 with endogenous WDR20 are assessed by IP and western blot upon co-transfection. All residues mutated in (C) and (D) can be found in (B).

long, winding loops, as well as three extra β strands that extend blades 4 and 7. WDR20 also differs from UAF1 by binding USP12 via a confined top surface area. Instead of using most of the top surface loops, WDR20 adheres to the enzyme with loops from only three adjacent blades. The WDR20-USP12 interface is centered on a row of three hydrophobic WDR20 residues, W306, F262, and Y261, which are further supported by their surrounding polar amino acid side chains and backbone groups. Consistent with an important role in binding USP12, mutations of W306 and F262 effectively abolish the ability of WDR20 to interact with and activate USP12 (Figures 4C and S4D).

The predominant USP12-WDR20 interface also involves major structural elements that are topologically connected to UAF1 binding in the UAF1-USP12 structures. These include the PK Helix, the PK Loop, the base of BL1, and a nearby long loop at the back of the Fingers domain, which we name the Backhand Loop (Figures 4A and 4B). Together, these USP12 regions pre-

sent a complementary surface with a string of hydrophobic residues in the middle to hold WDR20 in place. In USP1, the PK Loop features a unique ~20-amino acid insertion, which likely prevents USP1 from interacting with WDR20 (Figures S1A and S4C). Adjacent to the major USP12-WDR20 interface, the tip of USP12 BL3, which is otherwise disordered in both free and UAF1-bound forms of the enzyme, adopts a stable structure by making van der Waal contacts with WDR20. Mutations of residues at this peripheral interface (T351A and S352A of USP12 and N41 and E534 of WDR20) have little effect on complex formation, in contrast to the central interface (F287A and V279A of USP12 and W306 and F262 of WDR20) (Figures 4C and 4D).

Structural Features of UAF1-WDR20-Bound USP12

Binding of WDR20 to the UAF1-USP12 complex induces multiple structural changes in the enzyme, converting it into a compact form similar to Ub-bound USP46. The hallmark of these

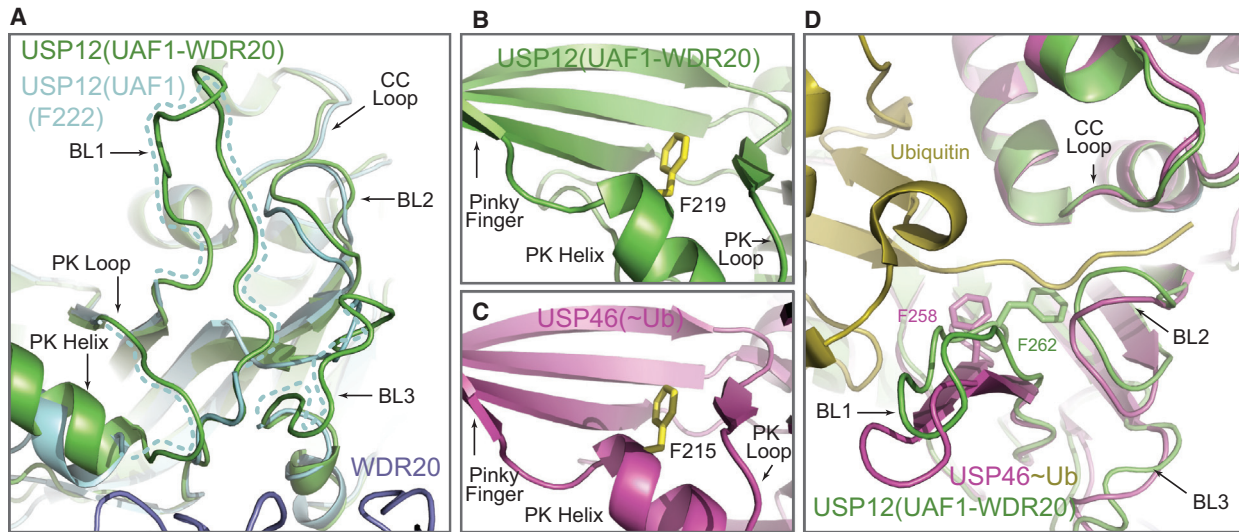


Figure 5. Structural Comparisons of Activator-Bound USP12 and Ub-Conjugated USP46

(A) Superposition of UAF1-bound USP12 and UAF1-WDR20-bound USP12 highlighting stabilization of BL1 and BL3 in the ternary complex.

(B and C) A comparison between the UAF1-WDR20-bound USP12 and the Ub-conjugated USP46 structures, focusing on the stabilized PK Loop, the regularized PK Helix, and the F219 residue at the Fingers-Palm domain junction.

(D) A close-up view of BL1 and the catalytic cleft of USP12 in complex with UAF1 and WDR20. The Thumb and Palm domains of Ub-conjugated USP46 are superimposed with their corresponding parts in USP12. The USP12 BL1 residue F262 is shown in sticks to highlight its blocking position.

changes is the stabilization of BL1 and a network of well-organized structural elements surrounding its base (Figure 5A). These elements include a regularized and relocated PK Helix, a structurally ordered PK Loop, and a rigidified BL3. While the Pinky Finger of USP12 in the UAF1-USP12-WDR20 complex adopts the same β strand conformation as seen in the UAF1-USP12 complex, F219 on the PK Helix becomes embedded in the pocket formed between the Fingers and the Palm domains, instead of being tucked underneath the Fingers domain (Figures 3D, 5B, and 5C). At the opposite end of the enzyme near the catalytic site, the catalytic cleft of USP12 adopts a closed conformation in the ternary complex, which is characterized by the well-ordered CC Loop opposing BL2 (Figure 5A). Overall, the UAF1-USP12-WDR20 complex is distinguished from the two free USP12 structures and the two UAF1-USP12 complex structures by the apparent stabilization of most flexible structural elements found in the DUB. Superposition analysis of Ub~USP46 and the UAF1-USP12-WDR20 structure shows that BL1 and BL2 of USP12 in the ternary complex are still in their “blocking” positions, just like in the free USP12 structure (Figures 1B and 5D). For example, in contrast to the USP46 BL1 residue F258, which supports the tail of Ub, the corresponding USP12 residue F262 is pushed into the catalytic cleft and would collide with the substrate.

Mechanism of USP12 Activation by UAF1 and WDR20

Using ubiquitin-7-amido-4-methylcoumarin (Ub-AMC) as a substrate, we have previously shown that UAF1 activates USP1 mainly by increasing its catalytic turnover (k_{cat}), instead of its affinity toward the substrate (K_m) (Cohn et al., 2007). To gain deeper mechanistic insights into USP12 activation by UAF1 and WDR20, we first determined the steady-state kinetics of

substrate hydrolysis by USP12 in different forms. Consistent with our results on USP1, activation of USP12-WDR20 by UAF1 is achieved mainly through an ~20-fold increase of k_{cat} with little change in K_m , suggesting that substrate affinity of USP12 is not altered by UAF1 (Figures 6A and S5A–S5D). A comparison between the activities of the UAF1-USP12 and those of the UAF1-USP12-WDR20 complex yielded a similar conclusion for WDR20, which also potentiates the enzyme by enhancing its k_{cat} . To validate these results, we used a Bio-Layer Interferometry-based direct-binding assay to compare the binding of a substrate mimetic to a USP12 active site mutant (C48S) with or without the two activators. In these assays, we replaced Ub-AMC with a Ub-peptide conjugate, Ub~(AKA), which contains a natural Ub-lysine isopeptide linkage imitating the physiological substrates of USP12 (Weller et al., 2014). In agreement with our enzyme kinetics data, our binding studies revealed negligible changes in the substrate binding affinity of USP12 induced by UAF1 or WDR20 (Figures 6A and S6). USP12 exhibits at least 25-fold higher affinity for the Ub~(AKA) conjugate than for Ub (Figure S5E), indicating that substrate binds USP12 tighter than the reaction product and that recognition of the isopeptide linkage by the catalytic cleft of USP12 is a major determinant of the substrate binding affinity.

Our kinetics and binding data have two important implications. First, our results rule out the possibility that UAF1 and WDR20 activate USP12 by enhancing its substrate affinity. With a binding site distant from the catalytic triad of USP12, these two proteins most likely modulate the enzyme through an allosteric effect that promotes catalytic efficiency. Second, contrary to what their names suggest, the BLs of USP12 do not impose steric hindrance to substrate binding. Although the structures of the inactive enzyme reveal a constricted catalytic cleft, the same

A

Sample	Ub-AMC		Ub~(AKA)
	k_{cat} (min ⁻¹)	K _M (μM)	K _D (μM)
USP12	n/a	n/a	9.1 ± 4.0
USP12-UAF1	1.6 ± 0.2	6.0 ± 1.5	5.8 ± 3.4
USP12-WDR20	0.6 ± 0.3	3.3 ± 0.7	8.4 ± 4.1
USP12-UAF1-WDR20	14.1 ± 2.7	4.7 ± 1.2	4.0 ± 2.3

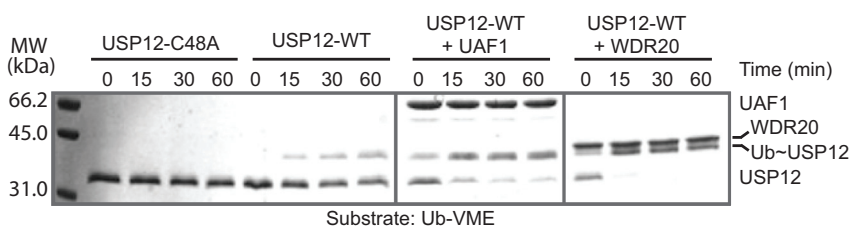
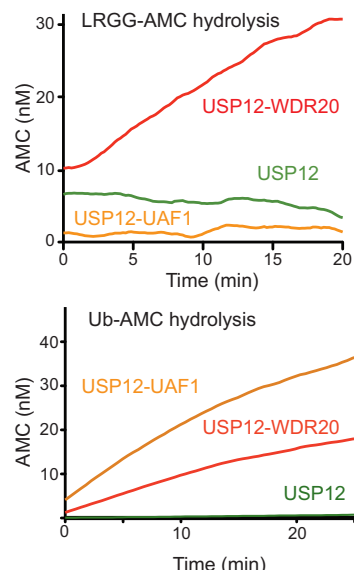
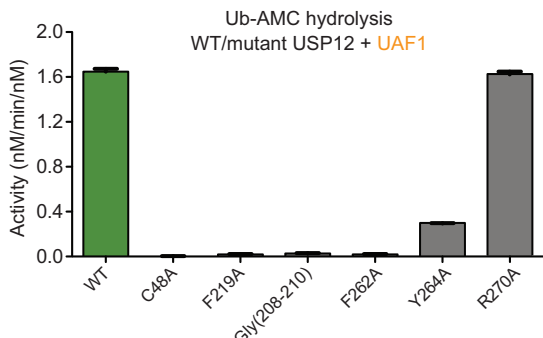
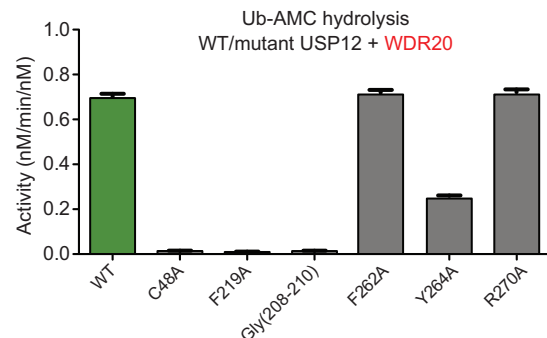
B**C****D****E**

Figure 6. Biochemical Analysis of USP12 Activation by UAF1 and WDR20

(A) Enzyme kinetics analyses of free and activator-bound USP12 with Ub-AMC substrate and binding analysis of a Ub~(AKA) peptide to all forms of USP12, as measured by an Octet Bio-Layer Interferometry system. The k_{cat} and K_M values are presented as means ± SD (n = 3), and the K_D values were obtained through steady-state analysis (see [Supplemental Experimental Procedures](#) for technical discussion).

(B) Time course of USP12 modification by the suicidal Ub-VME substrate in the absence or presence of UAF1 and WDR20.

(C) Time course of LRGG-AMC (top) in contrast to Ub-AMC (bottom) hydrolysis by USP12 (green), UAF1-USP12 (orange), and USP12-WDR20 (red). The LRGG-AMC hydrolysis reactions include a 100 μM substrate and a 10 μM enzyme.

(D and E) Rates of Ub-AMC hydrolysis by wild-type (WT) and mutant USP12 in the presence of UAF1 (D) or WDR20 (E). Mutations of the catalytic Cys48 residue and Arg270, which is not predicted to contact Ub, are used as controls. F219 is the PK Helix residue located at the Fingers-Palm domain junction. Gly(208–210) represents a mutant with amino acids 208–210 in the PK Loop mutated to glycine. Residues Phe262, Tyr264, and Arg270 on BL1 can be found in [Figure S5F](#).

feature is observed in its fully activated form with both UAF1 and WDR20 bound. The largely constant substrate affinity of USP12 in different forms negates a role of the BLs in controlling the accessibility of the Ub-binding surface of the enzyme. Conceivably, these loops have a certain degree of structural plasticity and can sample both closed and open conformations in the absence of the substrate. Such plasticity is detected crystallographically for BL2 and the CC Loop in our two UAF1-USP12 structures. Consistent with this concept, we found that the catalytic site of free USP12 can be modified by a suicidal substrate, Ub-VME (Ub-vinyl methyl ester), whose action requires full access to the catalytic cleft ([Figure 6B](#)). Both UAF1 and WDR20 can accelerate this modification reaction. Without increasing

substrate affinity, they most likely potentiate USP12 by promoting the step of nucleophilic attack by the catalytic cysteine.

Dissection of the Allosteric Pathways

The distinct binding sites and synergistic effect of the two propeller proteins on USP12 raise the question of whether UAF1 and WDR20 activate USP12 via two independent or converging allosteric pathways. Our structures seem to suggest BL1 is the common allosteric impact site for the two activators with opposite effects. In the two UAF1-USP12 complex structures, UAF1 binding appears to induce BL1 destabilization via a chain of conformational changes, whereas the WDR20-USP12 interaction seems to overwrite the allosteric effect of UAF1 by

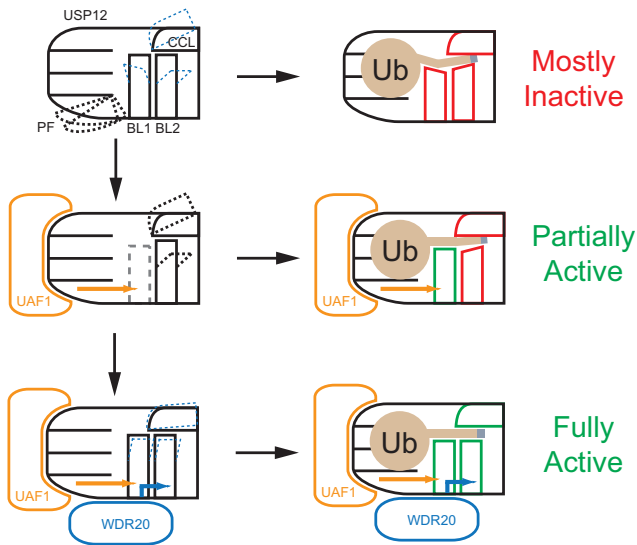


Figure 7. A Schematic Model of USP12 Activation by UAF1 and WDR20

Cartoon representations of the right-hand-shaped free and activator-bound USP12 and their substrate-bound forms. Key structural elements, including Pinky Finger (PF), BL1, BL2, and CC Loop (CCL), are labeled. Thick dotted black lines represent crystallographically observed alternative conformations. Thin dotted blue lines represent anticipated flexible conformations of the relevant structural elements. Solid red lines indicate structural elements with suboptimal conformation for catalysis. Solid green lines represent structural elements optimized for enzyme activity. Arrowed lines indicate transmission of allosteric effects induced by activator binding. A gray block at the end of the Ub tail indicates the isopeptide bond linkage. Free USP12 is characterized by its structurally flexible Pinky Finger, BLs, and possibly CCL, which allow full access of the catalytic cleft to a Ub-conjugated substrate. However, the free enzyme is inactive, mostly likely due to the non-productive conformations of BL1, BL2, and CCL. UAF1 and WDR20 binding allosterically regulate the topology of BL1 and the catalytic cleft, respectively. In all cases, substrate binding stabilizes BL1, BL2, and CCL. Their optimal conformations are conferred by the allosteric effects elicited by the activating proteins.

restabilizing the loop. To dissect the allosteric pathways for the two activators, we first repeated the substrate hydrolysis experiments with a peptide substrate, Leu-Arg-Gly-Gly (LRGG)-AMC, which contains only the extreme C-terminal four residues of Ub. In all Ub-bound USP structures, including Ub~USP46, this portion of the Ub tail is exclusively sandwiched by the CC Loop and BL2 but not by BL1 (Figure 1B). WDR20 was able to activate the enzyme to hydrolyze the peptide substrate, yet USP12 remained inactive toward LRGG-AMC in the presence of UAF1 (Figure 6C). Addition of a tail-less Ub did not rescue the activation activity of UAF1 (data not shown). These results strongly suggest that WDR20 can activate USP12 by allosterically optimizing its catalytic cleft, whereas the effect of UAF1 binding cannot be directly transmitted to the catalytic cysteine through USP12. Its propagation most likely requires optimal spatial configuration of the intact Ub substrate.

To further verify the independent allosteric mechanisms, we designed a series of USP12 mutations, focusing on BL1 and its surrounding regions, and tested their effects on enzyme activation by the two propeller proteins. With a mutation introduced to

the BL1 residue F262, USP12 could no longer be activated by UAF1 but retained full WDR20-stimulated activity (Figures 6D and 6E). In the Ub~USP46 structure, the corresponding USP46 residue F258 sits underneath the junction region between the Ub globular domain and its LRGG tail (Figures 1B and 5D). This result clearly indicates that UAF1 and WDR20 allosterically activate USP12 through two distinct pathways. Activation of USP12 by UAF1 requires structural fine-tuning at the junction of the Ub globular domain and its tail through BL1, whereas WDR20 acts independently of this site and directly affects the catalytic cleft. Even though BL1 of USP12 is collapsed in our UAF1-USP12 complex structures, Ub binding is expected to stabilize it via substrate-induced fit, as seen in other USPs and the Ub-conjugated USP46 structures. Therefore, complete destabilization of BL1 per se is not the ultimate effect of UAF1 binding for USP12 activation. UAF1 most likely makes a fine adjustment of Ub-stabilized BL1 to improve the catalytic competency of the enzyme. These notions are fully supported by both the critical role of the BL1 residue F262 in USP12 activation and the lack of activity in two additional USP12 mutants, where USP12 contains either an F219A mutation at the Fingers-Palm domain junction or a PK Loop with a flexible triple-glycine sequence (Figure 6D). Finally, consistent with the expected substrate-induced interactions between Ub and BL1 of USP12 in all forms, mutation of a Ub globular domain-binding residue on BL1, Y264, compromised the ability of both UAF1 and WDR20 to activate USP12 for Ub-AMC hydrolysis (Figures 6D, 6E, and S5F). As a control, alteration of a nearby solvent-exposed BL1 residue, R270, had little effect. These results suggest that even though fine-tuning the Ub globular domain-tail junction is not critical for WDR20 to activate USP12, interaction between BL1 and the Ub globular domain is still important for the full WDR20-stimulated USP12 activity.

DISCUSSION

The catalytic domains of USPs are characterized by their structural plasticity, which is highly susceptible to regulation. Our studies not only reveal the distinct binding modes of two activators of a single USP enzyme but also elucidate the allosteric nature of their effects and their independent allosteric pathways. Based on our results, we propose a tenable model for USP12 activation by UAF1 and WDR20 (Figure 7). Although our structures have captured free USP12 with a closed catalytic cleft, our biochemical data suggest that isolated USP12 is fully capable of engaging its substrate. The substrate-enzyme complex, however, is mostly inactive for two possible reasons. First, we speculate that upon substrate binding, BL1 of free USP12 might adopt a non-productive topology, leaving the tail of Ub in a distorted conformation incompatible for catalysis. Second, its catalytic cleft, demarcated by BL2 and the CC Loop, might be in a suboptimal form for catalyzing the hydrolysis reaction. UAF1 activates USP12 by binding to the tip of its Fingers domain and transmitting a long-range allosteric signal to BL1. Although BL1 is destabilized in the crystal structures of the UAF1-USP12 complex, it is expected to adopt a productive conformation upon substrate binding and play an important role in adjusting the topology of the Ub tail by fine-tuning its preceding

region. The DUB can be further activated by WDR20, which anchors at the base of BL1 but allosterically regulates the conformation of BL2 and the catalytic cleft. The allosteric effect of WDR20 binding is conceivably mediated by BL3, whose base is structurally coupled to the bases of both BL1 and BL2.

Given their strategic locations, the BLs of USPs have long been speculated for enzyme regulation (Hu et al., 2005). Our results provide the first lines of evidence for their direct involvement in enzyme activation mechanisms. To better reflect their role in modulating substrate configuration instead of the accessibility of the substrate-binding site, we propose renaming these loops as binding loops. We speculate that these loops and several other flexible structural elements identified in our studies play an important role in the activation of many other USP enzymes. USPs have emerged as a new class of promising therapeutic targets (Chauhan et al., 2012; Colland et al., 2009; Kapuria et al., 2010; Lee et al., 2010; Liang et al., 2014; Mistry et al., 2013; Tian et al., 2014). Most USP inhibitors, however, target the active site of USPs with limited specificity. Together with a recently reported specific and allosteric USP1-UAF1 small molecule inhibitor (Liang et al., 2014), our studies suggest that blocking the allosteric activation pathway might be an alternative strategy for discovering USP inhibitors with high specificity. Besides enzyme activation, UAF1 plays a crucial role in substrate recruitment. Such a dual role of a USP activator further expands the opportunities for developing USP-specific antagonists through substrate binding disruption.

EXPERIMENTAL PROCEDURES

Protein Purification, Crystallization, and Structural Determination

The human USP12 and WDR20 were expressed in *Escherichia coli* cells. The human UAF1 or UAF1-USP12 complex was expressed and purified from Hi5 insect cells. The UAF1ΔSLD-WDR20-USP12 complex was prepared by mixing the UAF1ΔSLD-USP12 complex with proteolytically treated WDR20. All crystals were obtained by the hanging-drop vapor diffusion method. All datasets were collected at the Advanced Light Source beamlines. Reflection data were processed with the HKL2000 package (Otwinowski and Minor, 1997). The UAF1-USP12 structure was determined with a combination of molecular replacement (MR) and single-wavelength anomalous diffraction methods. All other structures were determined by MR. Model building and refinement were performed using COOT and the PHENIX package (Adams et al., 2002; Collaborative Computational Project, Number 4, 1994). See Figure S7 for representative electron densities. See Supplemental Information for details.

In Vitro Deubiquitination Assay

Fluorescent enzymatic assays were performed by following the hydrolytic liberation of AMC from Ub-AMC (Boston Biochem) or LRGG-AMC. Measurements were performed in parallel in a final volume of 100 µl using 96-well half-area black plates with a 2300 Multilabel Reader (PerkinElmer). Assay results were analyzed with Prism 5.0 (GraphPad). For the Ub-VME (Boston Biochem) conjugation assays, proteins were incubated with Ub-VME at a molar ratio of 1:2 before SDS-PAGE analysis. See Supplemental Information for details.

In Vitro Binding Assays

Binding affinities of the Ub~(AKA) peptide to free and activator-bound USP12C48A mutant were measured using Octet RED96 (ForteBio, Pall). The data were analyzed with the Octet data analysis software. The association and dissociation curves were fit with a 2:1 heterogeneous ligand model, which might reflect two different conformational species of the enzyme or the two distinct steps of Ub~(AKA) binding involving the Ub globular domain and the isopeptide linkage. The $R^{Equilibrium}$ values were used to calculate the dissociation

constant K_D with steady-state binding analysis. Isothermal calorimetry (ITC) experiments were performed using a VP-ITC calorimeter (Microcal) and analyzed with Microcal ORIGIN software. See Supplemental Information for details.

Cell Culture, Antibodies, and Co-immunoprecipitation

293T cells were cultured following standard culture conditions and procedures. Human USP1, USP12, and UAF1 cDNAs were ligated to the pcDNA3.1 vector (Clontech Laboratories) modified with N-terminal Myc, hemagglutinin (HA), and FLAG peptides, respectively. Cellular lysates were resolved by NuPAGE (Invitrogen) gels and transferred onto polyvinylidene fluoride membrane (EMD Millipore), followed by immunoblotting using antibodies as indicated. Co-immunoprecipitation was performed with anti-FLAG M2 affinity gel or anti-Myc agarose affinity gel (Sigma). See Figure S7 for all full, uncropped western blot scans. See Supplemental Information for details.

ACCESSION NUMBERS

The accession numbers for the coordinates and structure factors reported in this paper are PDB: 5K16, 5K1B, 5K1A, 5K19, and 5K1C for free USP12, UAF1-USP12 (F222 space group), UAF1-USP12 (C2 space group), WDR20, and UAF1-USP12-WDR20, respectively.

SUPPLEMENTAL INFORMATION

Supplemental Information includes Supplemental Experimental Procedures, seven figures, and one table can be found with this article online at <http://dx.doi.org/10.1016/j.molcel.2016.05.031>.

AUTHOR CONTRIBUTIONS

H.L., N.Z., and A.D.D. conceived and H.L. conducted the protein crystallization experiments. H.M. and J.S. provided suggestions to protein purification. H.L. and N.Z. determined and analyzed the structures. C.E.W. and C.C. designed and synthesized Ub~(AKA). T.R.H. and H.L. conducted substrate binding and substrate hydrolysis experiments. H.L., H.K., K.S.L., A.D.D., and N.Z. conceived and H.K., U.J., and K.S.L. conducted cell-based mutational analyses. H.L., A.D.D., and N.Z. wrote the manuscript with inputs from all authors.

ACKNOWLEDGMENTS

We thank the beamline staff of the Advanced Light Source at Lawrence Berkeley National Laboratory. We also thank members of the N.Z. and Wenging Xu laboratories for discussion and help. This work is supported by the Wong Family Award (K.S.L.), the Howard Hughes Medical Institute (N.Z.), and NIH (R01GM110430 to C.C. and R01DK43889 and R37HL052725 to A.D.D.)

Received: April 12, 2016

Revised: May 12, 2016

Accepted: May 20, 2016

Published: June 30, 2016

REFERENCES

- Adams, P.D., Grosse-Kunstleve, R.W., Hung, L.W., Ioerger, T.R., McCoy, A.J., Moriarty, N.W., Read, R.J., Sacchettini, J.C., Sauter, N.K., and Terwilliger, T.C. (2002). PHENIX: building new software for automated crystallographic structure determination. *Acta Crystallogr. D Biol. Crystallogr.* 58, 1948–1954.
- Avvakumov, G.V., Walker, J.R., Xue, S., Finerty, P.J., Jr., Mackenzie, F., Newman, E.M., and Dhe-Paganon, S. (2006). Amino-terminal dimerization, NRDP1-rhodanese interaction, and inhibited catalytic domain conformation of the ubiquitin-specific protease 8 (USP8). *J. Biol. Chem.* 281, 38061–38070.
- Burska, U.L., Harle, V.J., Coffey, K., Darby, S., Ramsey, H., O'Neill, D., Logan, I.R., Gaughan, L., and Robson, C.N. (2013). Deubiquitinating enzyme Usp12 is a novel co-activator of the androgen receptor. *J. Biol. Chem.* 288, 32641–32650.

- Chauhan, D., Tian, Z., Nicholson, B., Kumar, K.G., Zhou, B., Carrasco, R., McDermott, J.L., Leach, C.A., Fulciniti, M., Kodrasov, M.P., et al. (2012). A small molecule inhibitor of ubiquitin-specific protease-7 induces apoptosis in multiple myeloma cells and overcomes bortezomib resistance. *Cancer Cell* 22, 345–358.
- Cohn, M.A., Kowal, P., Yang, K., Haas, W., Huang, T.T., Gygi, S.P., and D'Andrea, A.D. (2007). A UAF1-containing multisubunit protein complex regulates the Fanconi anemia pathway. *Mol. Cell* 28, 786–797.
- Cohn, M.A., Kee, Y., Haas, W., Gygi, S.P., and D'Andrea, A.D. (2009). UAF1 is a subunit of multiple deubiquitinating enzyme complexes. *J. Biol. Chem.* 284, 5343–5351.
- Collaborative Computational Project, Number 4 (1994). The CCP4 suite: programs for protein crystallography. *Acta Crystallogr. D Biol. Crystallogr.* 50, 760–763.
- Colland, F., Formstecher, E., Jacq, X., Reverdy, C., Planquette, C., Conrath, S., Trouplin, V., Bianchi, J., Aushev, V.N., Camonis, J., et al. (2009). Small-molecule inhibitor of USP7/HAUSP ubiquitin protease stabilizes and activates p53 in cells. *Mol. Cancer Ther.* 8, 2286–2295.
- Dahlberg, C.L., and Juo, P. (2014). The WD40-repeat proteins WDR-20 and WDR-48 bind and activate the deubiquitinating enzyme USP-46 to promote the abundance of the glutamate receptor GLR-1 in the ventral nerve cord of *Caenorhabditis elegans*. *J. Biol. Chem.* 289, 3444–3456.
- Ernst, A., Avvakumov, G., Tong, J., Fan, Y., Zhao, Y., Alberts, P., Persaud, A., Walker, J.R., Neculai, A.M., Neculai, D., et al. (2013). A strategy for modulation of enzymes in the ubiquitin system. *Science* 339, 590–595.
- Faesen, A.C., Dirac, A.M., Shanmugham, A., Ovaa, H., Perrakis, A., and Sixma, T.K. (2011). Mechanism of USP7/HAUSP activation by its C-terminal ubiquitin-like domain and allosteric regulation by GMP-synthetase. *Mol. Cell* 44, 147–159.
- Gangula, N.R., and Maddika, S. (2013). WD repeat protein WDR48 in complex with deubiquitinase USP12 suppresses Akt-dependent cell survival signaling by stabilizing PH domain leucine-rich repeat protein phosphatase 1 (PHLPP1). *J. Biol. Chem.* 288, 34545–34554.
- Hecker, C.M., Rabiller, M., Haglund, K., Bayer, P., and Dikic, I. (2006). Specification of SUMO1- and SUMO2-interacting motifs. *J. Biol. Chem.* 281, 16117–16127.
- Hershko, A., and Ciechanover, A. (1998). The ubiquitin system. *Annu. Rev. Biochem.* 67, 425–479.
- Hu, M., Li, P., Li, M., Li, W., Yao, T., Wu, J.W., Gu, W., Cohen, R.E., and Shi, Y. (2002). Crystal structure of a UBP-family deubiquitinating enzyme in isolation and in complex with ubiquitin aldehyde. *Cell* 111, 1041–1054.
- Hu, M., Li, P., Song, L., Jeffrey, P.D., Chenova, T.A., Wilkinson, K.D., Cohen, R.E., and Shi, Y. (2005). Structure and mechanisms of the proteasome-associated deubiquitinating enzyme USP14. *EMBO J.* 24, 3747–3756.
- Huang, T.T., Nijman, S.M., Mirchandani, K.D., Galardy, P.J., Cohn, M.A., Haas, W., Gygi, S.P., Ploegh, H.L., Bernards, R., and D'Andrea, A.D. (2006). Regulation of monoubiquitinated PCNA by DUB autocleavage. *Nat. Cell Biol.* 8, 339–347.
- Joo, H.Y., Jones, A., Yang, C., Zhai, L., Smith, A.D., 4th, Zhang, Z., Chandrasekharan, M.B., Sun, Z.W., Renfrow, M.B., Wang, Y., et al. (2011). Regulation of histone H2A and H2B deubiquitination and *Xenopus* development by USP12 and USP46. *J. Biol. Chem.* 286, 7190–7201.
- Kapuria, V., Peterson, L.F., Fang, D., Bornmann, W.G., Talpaz, M., and Donato, N.J. (2010). Deubiquitinase inhibition by small-molecule WP1130 triggers aggresome formation and tumor cell apoptosis. *Cancer Res.* 70, 9265–9276.
- Kee, Y., Yang, K., Cohn, M.A., Haas, W., Gygi, S.P., and D'Andrea, A.D. (2010). WDR20 regulates activity of the USP12 × UAF1 deubiquitinating enzyme complex. *J. Biol. Chem.* 285, 11252–11257.
- Kim, H., and D'Andrea, A.D. (2012). Regulation of DNA cross-link repair by the Fanconi anemia/BRCA pathway. *Genes Dev.* 26, 1393–1408.
- Köhler, A., Zimmerman, E., Schneider, M., Hurt, E., and Zheng, N. (2010). Structural basis for assembly and activation of the heterotetrameric SAGA histone H2B deubiquitinase module. *Cell* 141, 606–617.
- Komander, D., Clague, M.J., and Urbé, S. (2009). Breaking the chains: structure and function of the deubiquitinases. *Nat. Rev. Mol. Cell Biol.* 10, 550–563.
- Lee, B.H., Lee, M.J., Park, S., Oh, D.C., Elsasser, S., Chen, P.C., Gartner, C., Dimova, N., Hanna, J., Gygi, S.P., et al. (2010). Enhancement of proteasome activity by a small-molecule inhibitor of USP14. *Nature* 467, 179–184.
- Lei, J., Mesters, J.R., Drosten, C., Anemüller, S., Ma, Q., and Hilgenfeld, R. (2014). Crystal structure of the papain-like protease of MERS coronavirus reveals unusual, potentially druggable active-site features. *Antiviral Res.* 109, 72–82.
- Li, X., Stevens, P.D., Yang, H., Gulhati, P., Wang, W., Evers, B.M., and Gao, T. (2013). The deubiquitination enzyme USP46 functions as a tumor suppressor by controlling PHLPP-dependent attenuation of Akt signaling in colon cancer. *Oncogene* 32, 471–478.
- Liang, Q., Dexheimer, T.S., Zhang, P., Rosenthal, A.S., Villamil, M.A., You, C., Zhang, Q., Chen, J., Ott, C.A., Sun, H., et al. (2014). A selective USP1-UAF1 inhibitor links deubiquitination to DNA damage responses. *Nat. Chem. Biol.* 10, 298–304.
- McClurg, U.L., Summerscales, E.E., Harle, V.J., Gaughan, L., and Robson, C.N. (2014). Deubiquitinating enzyme Usp12 regulates the interaction between the androgen receptor and the Akt pathway. *Oncotarget* 5, 7081–7092.
- Mistry, H., Hsieh, G., Buhrlage, S.J., Huang, M., Park, E., Cuny, G.D., Galinsky, I., Stone, R.M., Gray, N.S., D'Andrea, A.D., and Parmar, K. (2013). Small-molecule inhibitors of USP1 target ID1 degradation in leukemic cells. *Mol. Cancer Ther.* 12, 2651–2662.
- Moldovan, G.L., and D'Andrea, A.D. (2009). How the Fanconi anemia pathway guards the genome. *Annu. Rev. Genet.* 43, 223–249.
- Moretti, J., Chastagner, P., Liang, C.C., Cohn, M.A., Israël, A., and Brou, C. (2012). The ubiquitin-specific protease 12 (USP12) is a negative regulator of notch signaling acting on notch receptor trafficking toward degradation. *J. Biol. Chem.* 287, 29429–29441.
- Nijman, S.M., Huang, T.T., Dirac, A.M., Brummelkamp, T.R., Kerkhoven, R.M., D'Andrea, A.D., and Bernards, R. (2005a). The deubiquitinating enzyme USP1 regulates the Fanconi anemia pathway. *Mol. Cell* 17, 331–339.
- Nijman, S.M., Luna-Vargas, M.P., Velds, A., Brummelkamp, T.R., Dirac, A.M., Sixma, T.K., and Bernards, R. (2005b). A genomic and functional inventory of deubiquitinating enzymes. *Cell* 123, 773–786.
- Otwinski, Z., and Minor, W., eds. (1997). Processing of X-ray Diffraction Data Collected in Oscillation Mode (Academic Press).
- Ratia, K., Saikatendu, K.S., Santarsiero, B.D., Barretto, N., Baker, S.C., Stevens, R.C., and Mesecar, A.D. (2006). Severe acute respiratory syndrome coronavirus papain-like protease: structure of a viral deubiquitinating enzyme. *Proc. Natl. Acad. Sci. USA* 103, 5717–5722.
- Renatus, M., Parrado, S.G., D'Arcy, A., Eidhoff, U., Gerhardt, B., Hassiepen, U., Pierrat, B., Riedl, R., Vinzenz, D., Worpenberg, S., and Kroemer, M. (2006). Structural basis of ubiquitin recognition by the deubiquitinating protease USP2. *Structure* 14, 1293–1302.
- Reyes-Turcu, F.E., Ventii, K.H., and Wilkinson, K.D. (2009). Regulation and cellular roles of ubiquitin-specific deubiquitinating enzymes. *Annu. Rev. Biochem.* 78, 363–397.
- Samara, N.L., Datta, A.B., Berndsen, C.E., Zhang, X., Yao, T., Cohen, R.E., and Wolberger, C. (2010). Structural insights into the assembly and function of the SAGA deubiquitinating module. *Science* 328, 1025–1029.
- Sekiyyama, N., Ikegami, T., Yamane, T., Ikeguchi, M., Uchimura, Y., Baba, D., Ariyoshi, M., Tochio, H., Saitoh, H., and Shirakawa, M. (2008). Structure of the small ubiquitin-like modifier (SUMO)-interacting motif of MBD1-containing chromatin-associated factor 1 bound to SUMO-3. *J. Biol. Chem.* 283, 35966–35975.
- Song, J., Durrin, L.K., Wilkinson, T.A., Krontiris, T.G., and Chen, Y. (2004). Identification of a SUMO-binding motif that recognizes SUMO-modified proteins. *Proc. Natl. Acad. Sci. USA* 101, 14373–14378.

- Sowa, M.E., Bennett, E.J., Gygi, S.P., and Harper, J.W. (2009). Defining the human deubiquitinating enzyme interaction landscape. *Cell* 138, 389–403.
- Tian, Z., D'Arcy, P., Wang, X., Ray, A., Tai, Y.T., Hu, Y., Carrasco, R.D., Richardson, P., Linder, S., Chauhan, D., and Anderson, K.C. (2014). A novel small molecule inhibitor of deubiquitylating enzyme USP14 and UCHL5 induces apoptosis in multiple myeloma and overcomes bortezomib resistance. *Blood* 123, 706–716.
- Weller, C.E., Huang, W., and Chatterjee, C. (2014). Facile synthesis of native and protease-resistant ubiquitylated peptides. *ChemBioChem* 15, 1263–1267.
- Yang, K., Moldovan, G.L., Vinciguerra, P., Murai, J., Takeda, S., and D'Andrea, A.D. (2011). Regulation of the Fanconi anemia pathway by a SUMO-like delivery network. *Genes Dev.* 25, 1847–1858.
- Ye, Y., Scheel, H., Hofmann, K., and Komander, D. (2009). Dissection of USP catalytic domains reveals five common insertion points. *Mol. Biosyst.* 5, 1797–1808.
- Ye, Y., Akutsu, M., Reyes-Turcu, F., Enchev, R.I., Wilkinson, K.D., and Komander, D. (2011). Polyubiquitin binding and cross-reactivity in the USP domain deubiquitinase USP21. *EMBO Rep.* 12, 350–357.
- Yin, J., Schoeffler, A.J., Wickliffe, K., Newton, K., Starovasnik, M.A., Dueber, E.C., and Harris, S.F. (2015). Structural insights into WD-repeat 48 activation of ubiquitin-specific protease 46. *Structure* 23, 2043–2054.
- Zhang, X., Choi, P.S., Francis, J.M., Imielinski, M., Watanabe, H., Cherniack, A.D., and Meyerson, M. (2016). Identification of focally amplified lineage-specific super-enhancers in human epithelial cancers. *Nat. Genet.* 48, 176–182.